Hindawi
Journal of Sensors
Volume 2019, Article ID 5805609, 11 pages
https://doi.org/10.1155/2019/5805609

Research Article

Reduced Graphene Oxide Decorated with AuNPs as a New Aptamer-Based Biosensor for the Detection of Androgen Receptor from Prostate Cells

Bruno P. Crulhas, Caroline R. Basso, João P. R. L. L. Parra, Gustavo R. Castro, and Valber A. Pedrosa

Institute of Bioscience, Department of Chemistry and Biochemistry, UNESP, Botucatu, SP, Brazil

Correspondence should be addressed to Valber A. Pedrosa; vpedrosa@ibb.unesp.br

Received 5 November 2018; Revised 29 April 2019; Accepted 18 May 2019; Published 26 June 2019

Academic Editor: Roberto Paolesse

Here we described an aptasensor based on graphene oxide (GO) decorated with gold nanoparticles (AuNPs) able to detect the AR released by prostate cells, in order to provide new insights about the relationship between AR and prostate cancer for a more precise diagnosis for cancer. Characterization of the surface modified GE was carried out by cyclic voltammetry and electrochemical impedance spectroscopy using ferrocene as a redox probe. Under the optimized experimental conditions, a detection limit of 0.5 ng/mL (3σ/slope) was obtained by the present electrochemical biosensor, along with a linear range of 0-110 ng/mL. By virtue of excellent sensitivity, specificity, and repeatability, the present electrochemical biosensor provides a potential application in clinical diagnosis.

1. Introduction

The prostate cancer (PCa) is a worldwide health issue, being the most common cancer among men with approximately 15% of the global male population diagnosed with PCa at some point in their lifetime [1]. In addition, the mortality keeps increasing year by year due to the lack of an accurate early diagnostic procedure [2]; the gold standard technique relies only on invasive techniques such as the transrectal ultrasonography and tissue biopsy [3, 4]. The only biomarker used for screening exams is the prostate-specific antigen (PSA) [5]; however, PSA itself cannot provide reliable diagnosis for cancer detection and overexpression of it can be related to other prostate diseases rather than cancer [6, 7]. In this way, there are several reports in literature to find other suitable biomarkers for PCa detection and monitoring, such as vascular endothelial growth factor (VEGF) and polymorphic epithelial mucin type 1 (MUC1) [8, 9].

Recently, studies have started to be focused on the prostatic epithelial androgen receptor (AR) in order to better understand the PCa biochemical dynamics pathways [10–12]; the AR is a member of the nuclear steroid receptor family and its function is to regulate normal prostate growth by regulation factors that mediate the androgen action on prostate cells and is usually related to cellular proliferation [13]. However, in PCa, the AR is often related to increased capillary density within the tumor and it is also correlated with greater degree of tumor differentiation, promoting cancer progression as a proliferator factor or by stimulation of cancer progression [14, 15], being therefore an important biomarker for PCa therapeutic [16]. A series of new approaches, including polymerase chain reaction [17], bioluminescent [18], and capillary electrophoresis [19], have been developed for AR analysis. While these methods are powerful methodologies, they are not suitable to the in situ AR analysis of living cells due to their destructive procedures involving chemical labels and are time-consuming with complicated sample preparation and sophisticated instrumentation [20].

The discovery of graphene opened a new path to the development of novel sensing platforms [21], making it one of the most widely used materials for biosensors applications. The graphene oxide (GO) is a two-dimensional material with carbon atoms ordered in a honeycomb structure with unique structural, optical, thermal, and electronic properties

such as the quantum Hall effect, optical transmittance and fluorescence quenching ability, and high electron mobility [22, 23]. In addition, GO has high thermal conductivity; due to such features, the graphene nanocomposite is novel and powerful platform for sensors, super capacitors, and electrocatalysis application; moreover, it can be applied in order to develop transparent conductive films and electronic devices [24–26].

The combination of GO with metallic nanoparticles provides novel nanocomposites for a broad range of applications; for example, in the biosensing field such nanocomposites can overcome the actual limitations of sensing platforms by providing higher effective surface area, excellent catalytic properties, higher specificity, and lower limit of detection at nanoscale [27, 28]. In this way, the combination of graphene with metallic nanoparticles has already been exploited for developing an optical electrochemical biosensor for detection of several environmental pollutants [29, 30] and for cancer biomarkers [31, 32]. These metallic nanoparticles include palladium [33], antimony [34], silver [35], and gold [36], due to their enhanced characteristics [37]. In this way, the gold nanoparticles (AuNPs) are a powerful candidate to be conjugated with graphene, because it is a noble product with unique characteristics of biocompatibility, low toxicity, electrical features, and catalytic and surface-enhanced Raman properties; moreover, the AuNPs can be easily modified with biological samples (for example, nucleic acids (DNA or RNA), proteins, enzymes, and antibodies) making them a robust platform to be used for immunoassays, thermotherapy, hormones, pesticides, proteins, and virus and bacteria detection [38–40].

Hence, there is an increasing attention to DNA biosensors as a tool for cancer diagnosis and monitoring [41]. The use of aptamer-based sensors using gold electrodes in order to detect cancer biomarkers is well exploited in literature for a range of applications, such as early cancer detection, cancer monitoring, and drug delivery systems [8, 9, 42]. The combination of aptamer, rGO, and AuNPs is novel tendency for developing more powerful platforms, where the DNA immobilization can be enhanced by AuNPs offering higher surface area at nanoscale which increases the sensor sensitivity and also improves the electronic properties of the biosensor [21]. To better understand the AR protein patterns as marker for cancer monitoring, we described a novel graphene oxide decorated with AuNPs electrochemical aptamer-based biosensor able to detect the AR released by prostate cells in order to provide new insights about the relationship between AR and PCa for a more precise diagnosis and cancer. The biosensor was based on the self-assembly of thiolated aptamers tagged with methylene blue (MB) as redox label on AuNPs attached to reduced graphene oxide. When the AR binds to the aptamer, the DNA hairpin changes its configuration, leading to a reduction of the electron transfer.

2. Materials and Methods

2.1. Materials and Reagents. Glassy carbon electrode (GC), phosphate-buffered saline (PBS), gold (III) chloride trihydrate ($HAuCl_4$) 99.99%, 6-mercapto-1-hexanol (MCH), ferrocene (Fc), mucin 1 (MUC1), sodium dodecyl sulphate (SDS), sodium borohydride, bovine serum albumin (BSA), graphene oxide (GO), androgen receptor human (AR), and prostate-specific antigen (PSA) from human semen were purchased from Sigma-Aldrich (St. Louis, MO).

Trypsin-EDTA, cell culture medium RPMI 1640 (1×, with L-glutamine; VWR), fetal bovine serum (FBS), L-glutamine, and penicillin/streptomycin were purchased from Gibco® (Waltham, MA). Androgen receptor (AR) aptamer sequence was selected by previous reports in literature and the mechanism for changing the electrochemical signal is based on structure-switching [43] and it was provided by Biosearch Technologies (Novato, CA) and used as follows:

AR: 5′-SH/-5′-ACG-CTC-GGA-TGC-CAC-TAC-AGG-TTG-GGG-TCG-GGC-ATG-CGT-CCGG-3′-/MB.

2.2. Synthesis of rGO-AuNPs Composite. The rGO-AuNPs composite was synthesized accordingly to Donini et al. [23], with minor modifications. Briefly, a ratio by weight of 10:4 GO/SDS was dissolved in 3 mL of ethanol and the solution was sonicated for 20 min. Afterward, 2.6 mg of sodium borohydride was added and the solution was sonicated for 20 min; finally, a 1 mL solution containing 1 mg of $HAuCl_4$ was slowly added under constant stirring to the rGO solution; the remaining sodium borohydride acted as reducing agent for $HAuCl_4$; and after complete reduction of gold, the rGO-AuNPs solution was dispersed by ultrasonic probe for 1 h. The rGO-AuNPs obtained were centrifuged for 15 min at 10000 rpm and washed several times with ethanol. After that, 3 mL of ethanol was added to the remaining composite and it was dried at 60°C. The chemical synthesis of rGO was also performed, but without adding $HAuCl_4$, to evaluate the effects of AuNPs over rGO structure.

2.3. Development of the Aptamer-Based Sensors. AR aptamer was synthesized by Biosearch Technologies with a C6 disulfide linker at 5′-end with the intention to bind it to AuNPs at 3′-end; the MB was coupled to it in order to act as redox probe for electrochemical analysis. The AR aptamer stock solution was diluted in 50 mM using 10 mM of PBS buffer (pH 7.4), according to the manufacturer's protocol.

Prior to the rGO-AuNPs modification, the GC electrode was polished with 0.3 μm alumina slurries, rinsed with ultrapure distilled water, and sonicated for 30 min in ethanol, followed by electrochemical cleaning by 25 cycles 50 mV/s of cyclic voltammetry in 1m of $H2SO_4$ in potential ranging from -1.0 to 1.0 V. Afterward, a solution containing 0.2 mg of rGO-AuNPs composite and 1 mL of water was dispersed using ultrasonic for 30 min and 10 μL of this solution was added onto the surface of GC electrode and dried at 60°C; in order to compare the effects of adding AuNPs, the GC-rGO electrode was prepared as described above, but using 0.2 mg of rGO and 1 mL of water.

Aptamer immobilization was prepared by incubation of 1 μM of it on the surface of GC-rGO-AuNPs electrode for 18 h, in the dark, at 4°C (Figure 1). Afterward, the electrodes were immersed in 3 mM of MCH aqueous solution for 30 min to remove nonspecifically adsorbed molecules and passivate the

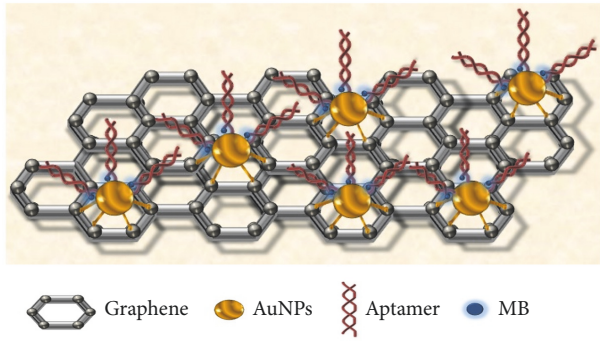

Figure 1: Scheme of the GC-rGO-AuNPs aptamer-based biosensor.

electrode surface through the backfilling method; for every step the electrodes were washed with PBS to remove the excess of reagents.

2.4. Prostate Cell Culture. Human prostate normal cells (PNT2; ECACC-95012613) and androgen-sensitive human prostate cancer cells (LNCaP; ATCC® CRL-1740™) were cultivated and used in the same way as previously reported by our group [43]. These two lineages were chosen to improve AR comparisons between cancer cells and normal prostate cells. Briefly, the cells were cultivated in 75 cm^2 flasks containing RPMI media, supplemented with FBS, L-glutamine, and penicillin/streptomycin. Cells were cultivated until 90% of confluence, after they were trypsinized using trypsin-EDTA. Cell viability was assessed through the Neubauer chamber count technique and approximately 10^5 cells were used in all experiments.

2.5. Electrochemical Characterization of the Aptamer-Based Sensors. Aptamer-based electrochemical sensors were characterized by scanning electron microscopy (SEM) using a Quanta 200 (FEI Company) coupled to an energy-dispersive X-ray spectroscopy analyzer (EDS) to analyze the dispersion of rGO-AuNPs layer on the surface of GC electrode. Electrochemical characterization was done in a μAutolab III/FRA2 (Metrohm, NL) potentiostat, using a three-electrode system, which consisted of Ag/AgCl (3 M KCl), as reference electrode; Pt wire, as auxiliary electrode; and GC, as working electrode. Characterization experiments were performed by cyclic voltammetry (CV) and electrochemical impedance spectroscopy (EIS). CV characterization of biosensor was done in a set of experiments; first a CV of GC-AuNPs and GC-rGO-AuNPs was done to verify signal gain from the addition of graphene to the sensing platform; after that a CV scan was performed using GC-rGO-AuNPs from 0.7 to -0.2V at several scan rates (20, 30, 50, 60, 90, 100, 150, 200, and 250 mV/s); EIS experiments were done to evaluate charge transfer resistance in each step of biosensor fabrication with a frequency range of 0.001 Hz to 10000 kHz in a 10 mM PBS solution (pH 7.2); and all experiments were done in triplicate.

2.6. AR Electrochemical Characterization, Calibration Curve, and Detection from Prostate Cells. Electrochemical cells consisted of suitable glass vessels of 2 mL where all electrodes could be easily submerged in the solution. The biosensor's operating strategy relies on the unfolding of hairpin structure of the aptamer upon binding the specific target; in this case the AR protein, the complex aptamer-protein binding, drastically changes the DNA conformation leading to a decrease in the efficiency of electron transfer from MB to working electrode surface reducing the peak. In order to evaluate the signal difference, the square wave voltammetry (SWV) was the technique utilized, at 40 mV amplitude and 60 Hz frequency ranging from 0.0 to -0.5 V; and due to its fast analysis, it was able to get measurements in a very short time difference (~1 min). Aptamer-based sensor was allowed to equilibrate through stable faradaic current, in order to enable AR characterization and detection.

The AR aptamer calibration curve was done by adding the recombinant target protein at known concentrations into the electrochemical cells after the stabilization of background current. The sensor was allowed to react with analyte for 20 min, before each measurement; signal loss was checked by SWV and converted into percentage of signal suppression (SS). All measurements were carried out in triplicate and the limit of detection (LOD) was calculated through linear regression by using the standard deviation of the y-intercept (LOD = 3σ/Slope). Moreover, in order to evaluate the biosensor specificity, analysis of interfering compounds was performed by SWV at 40 mV amplitude signal and frequency 60 Hz at the range -0.50 to 0.7 V versus Ag/AgCl reference; the interfering compounds chosen were 50 ng/mL of MUC1, 50 mg/mL of PSA, and 50 ng/mL of BSA. MUC1 and PSA were selected because they are also released by PCa cells and BSA due to its presence on cell culture media.

Finally, after the characterization and calibration, the aptamers-based sensor was applied to detect AR releasing patterns from different human prostate cells lineages (normal cell and cancer cell); electrochemical detection followed the same procedures described above, with minor modifications. Therefore, the electrochemical cells containing the oligo structures were kept under 5% CO_2, 95% air humidity atmosphere, at 37°C. The SWV at 40 mV amplitude signal and frequency 60 Hz at the range -0.50 to 0.7 V versus Ag/AgCl reference measurements were taken every 20 min, for 3 h, after cell incubation.

3. Results and Discussion

The biosensor consisted of reduced graphene oxide decorated with gold nanoparticles combined with aptamer tagged with methylene blue. The idea of using graphene combined with AuNPs relies on their properties, whereupon nanoparticles with size ranging from 1 to 100 nm can be used for cancer diagnosis and therapy at early stages; moreover the unique mechanical, electrical, and optical features demonstrate enhanced potential in developing novel platforms to detect cancer biomarkers [44]. In addition to rGO-AuNPs, the methylene blue is a redox molecule widely used in aptamer-based biosensors because it can be easily conjugated with DNA molecules [5, 6].

In order to characterize the electrochemical behavior of the biosensor, a CV was done to ensure whether the addition of graphene to AuNPs modified GC electrode could enhance the signal of the sensor. Figure 2(a) shows a 2-fold increasing in signal from electrode modified with graphene and AuNPs, ensuring the possibility of miniaturization and detection of AR in complex media due to graphene properties [21, 23]. Following electrochemical characterization of the biosensor, GC-rGO-AuNPs electrode was used for a set of experiments using CV in 10 mM PBS with 0.5 mM of Fc at scan rates ranging from 20 to 250 mV/s. The results demonstrated a gradual increase of the redox peak current to around 350 and 200 mV for cathodic and anodic peaks, respectively (Figure 2(b)), indicating the feasibility of the sensor to be used as working electrode. In addition, the correlation of redox peak currents with the scan rate is shown in Figure 2(c); redox peak currents were proportional to the square root of the scan rate ($v^{1/2}$), indicating a diffusion-controlled process. The reaction mechanism of the biosensor was analyzed by plotting peak potential versus scan rate, and the peak-to-peak separation (ΔEp) remained nearly constant up to 60 mV, which suggests the electrochemical process is reversible and confined by the surface of the GC-rGO-AuNPs electrodes (Figure 2(d)).

In addition to cyclic voltammetry characterization, electrochemical impedance spectroscopy (EIS) experiments were performed to evaluate the resistance of charge transfer in each step of the sensor assembly. Figure 2(d) shows a typical Nyquist plot of impedance recorded in a frequency range of 0.001 Hz–10000.0 Hz in 10 mM PBS (pH 7.2) containing 0.5 mM Fc. The semicircle diameter represents the electron-transfer kinetics which can be converted into the charge transfer resistance (R_{ct}) at the electrode surface. Figure 2(e) shows the EIS spectra on a step-by-step modification of the GC electrode with graphene coating; the electron-transfer resistance (R_{ct}, semicircle diameter) was 11 KΩ for bare GC electrode (green triangles). After addition of AuNPs, the resistance increased to 30 kΩ (red circles), demonstrating an enhanced resistance of electron transfer due to the rGO layer formed on top of the GC electrode; however, the combination of rGO with of AuNPs decreased the resistance down to 16 KΩ (black squares). This can be explained by the addition of graphene to the AuNPs, which improved the electrocatalytic current density of the nanocomposites by the high surface area, and rapid electron transport capability leads to the higher current value in comparison with unmodified electrode [45]. The next step was the addition of aptamer on the rGO-AuNPs by chemistry conjugation using the gold-thiol bonds and the MCH to passivate layer, which is a well-known modification for electrochemical aptamer-based biosensors [8, 9]. Such modifications on the nanocomposite layer slightly increased the resistance up to 26 kΩ (blue triangles). The final step was the addition of the target protein (pink diamonds), which increased the resistance to 37 kΩ, demonstrating in this way the binding affinity of the sensor to AR due to the attachment of protein molecules on the surface of the GC-rGO-AuNPs sensor, leading to an enhanced resistance on the electro transfer.

The electrochemical behavior of rGO-AuNPs aptamer was assessed by SWV by using MB as redox probe. The MB redox tag is widely used for the development of electrochemical-based aptamers [46, 47] and the stability of this novel nanocomposite was assessed through SWV (Figure 3(a)) in a buffer for 2 hours in 10 mM PBS (pH = 7.2). The sensor was highly stable with a signal loss of 13% at the end of the experiment (Figure 3(b)); such background signal is in accordance with similar results for a whole range of electrochemical aptamer-based biosensors, which used bare gold electrode as substrate for aptamers attachment, demonstrating the possibility of using graphene oxide decorated with AuNPs in order to provide new and more robust nanomaterials on biosensing field [8, 9, 47]. Moreover, the SEM image used in order to characterize the electrode's surface demonstrates a well formed layer with clusters of AuNPs, and the EDS scan corroborates the presence of carbon and gold in the electromagnetic emission spectrum (Figure 3(c)).

The calibration curve for GC-rGO-AuNPs-aptamer sensor was performed after all the characterization and optimization procedures. Detection limit and the linear detection range of AR were calculated by adding known concentrations of AR recombinant protein to the electrochemical cells (from 2 ng/mL to 110 ng/mL). Figure 4(a) depicts the SWV of the AR calibration curve and Figure 4(b) presents the signal decrease caused by the binding of target protein to the aptasensor. The signal suppression was calculated as $\Delta I = Ipb - Ipa$, wherein ΔI is the change in current, *Ipb* is the peak current before protein incubation, and *Ipa* is the peak current after protein incubation and it was converted into percentage of signal loss. AR signal suppression (SS) (Figure 4(b)) increased linearly with the increasing of AR concentration (SS = 9.23 x - 7.535 (R^2 = 0.99)). Detection limit found was calculated around 0.5 ng/mL with a linear range from 0 to 110 ng/mL; such range for detection is lined up with AR concentrations on human prostate tissue demonstrating the possibility of using the rGO-AuNPs-aptamer sensor in order to detect AR on biological samples [48].

The specificity of the rGO-AuNPs sensor to AR was evaluated by using common molecules found in body physiological conditions, such as PSA and MUC1. The BSA was also evaluated due to its presence in cell culture media, in order to mimic the cellular microenvironment [49]. Figure 4(c) demonstrates the similarity of SS for BSA, PSA, and MUC1 signal suppression and it can be comparable with background

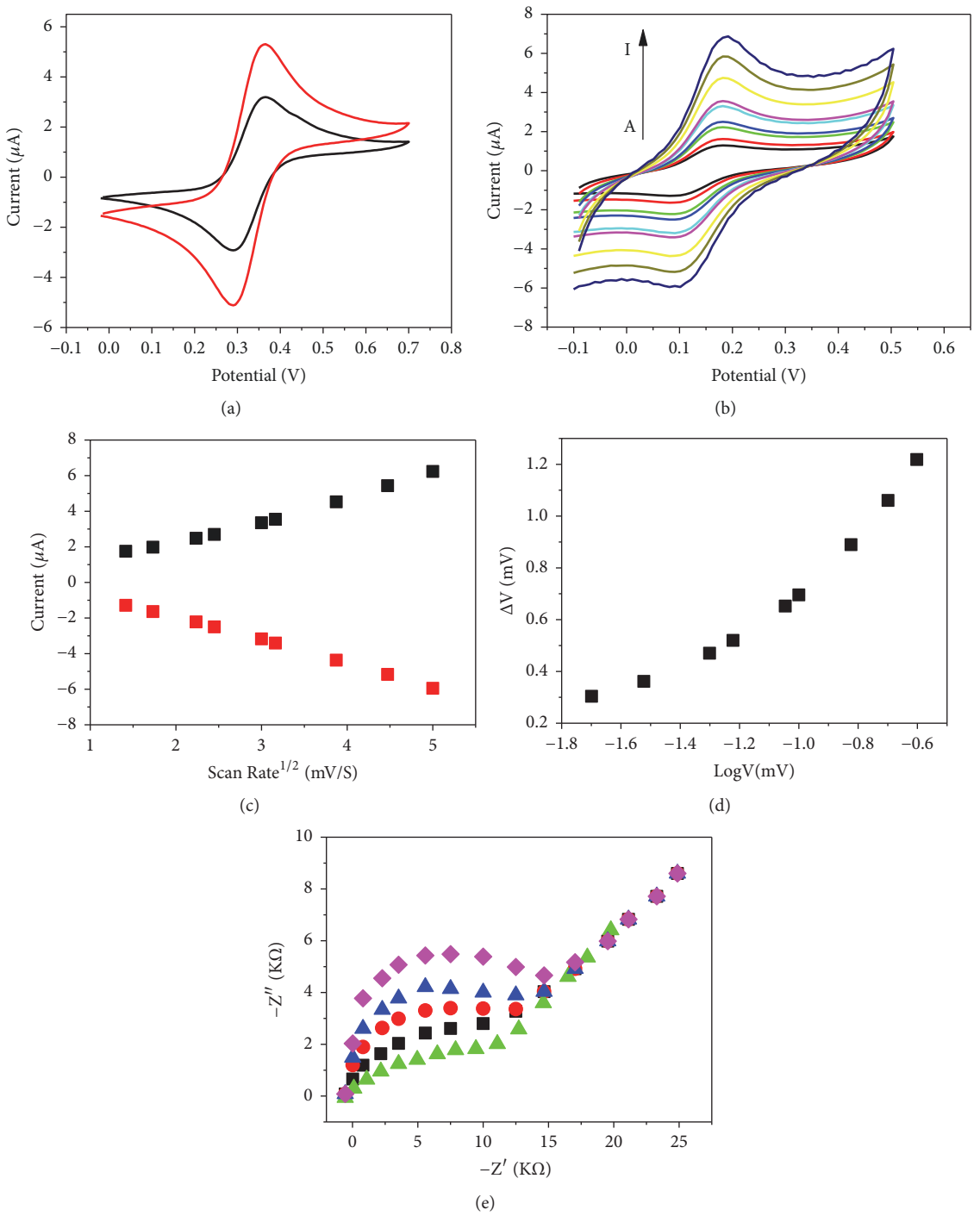

Figure 2: (a) Cyclic voltammograms of GC electrode with AuNPs (black line) and AuNPs conjugated with graphene (red line) in 0.1 M PBS buffer (ph 7.4). (b) Cyclic voltammograms of GC-rGO-AuNPs electrode at different scan rates (A–I: 20, 30, 50, 60, 90, 100, 150, 200, and 250 mV/s) in 0.1 M PBS buffer (pH 7.4). (c) Plot of redox peaks current versus square root of scan rate, cathodic peak (black square), and anodic peak (red square). (d) Peak-to-peak separation as a function of the potential scan rate. (e) Impedance spectroscopy GC-rGO-AuNPs electrodes. Nyquist plots for PEG-Au electrodes containing bare GC electrode (black square), GC-rGO (red circle), GC-rGO-AuNPs (green triangle), MCH backfilling (blue triangle), and GC-rGO-AuNPs (pink diamond) in the presence of 50 ng/mL of recombinant protein. Frequency intervals were from 0.001 Hz to 10000.0 Hz.

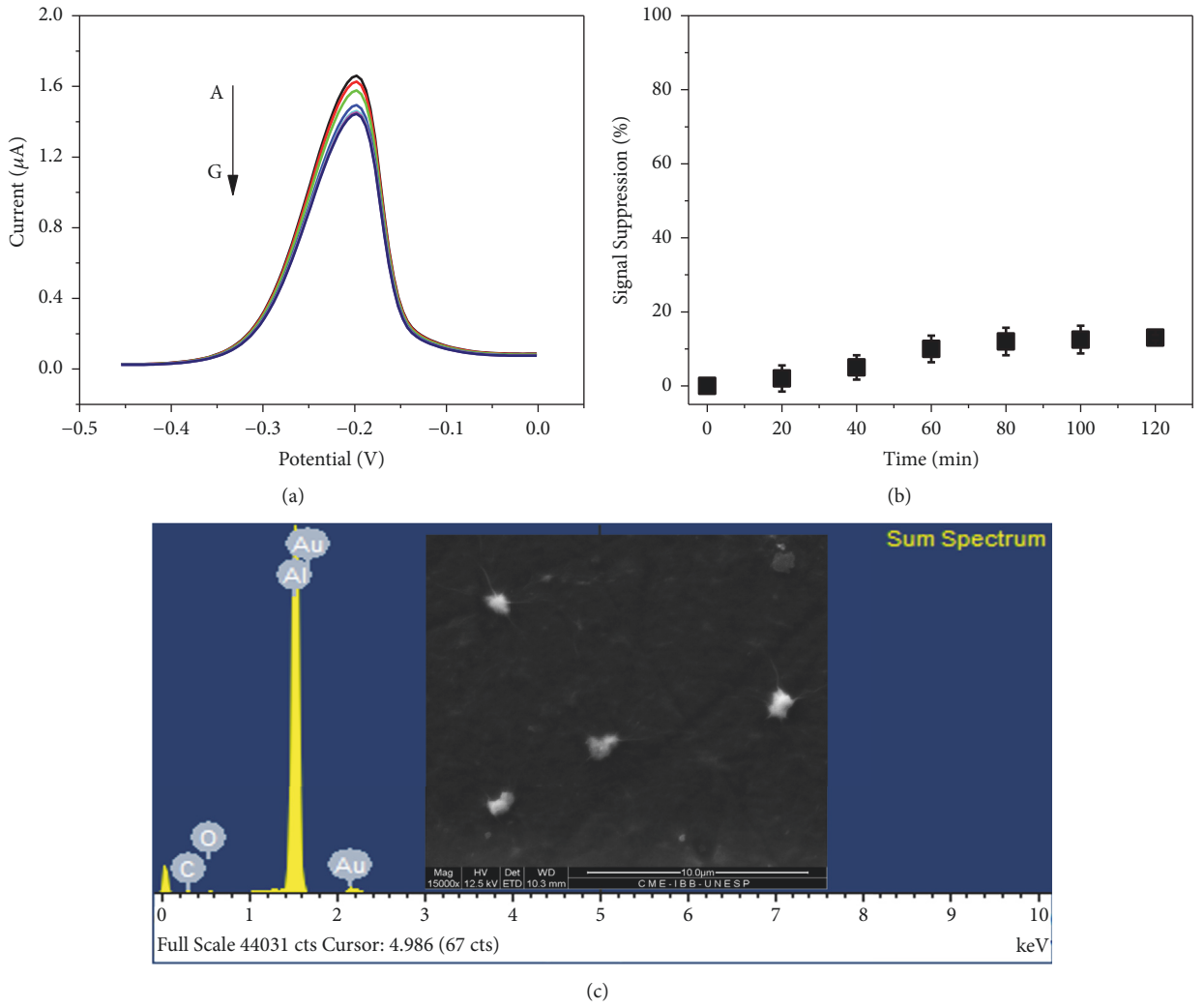

FIGURE 3: AR aptasensor stability. (a) SWV of AR aptasensor stabilization over time (A-G: 0, 20, 40, 60, 80, 100, and 120) at potential range from 0.0 to -0.5 V, at 40 mV amplitude, and frequency 60 Hz in 10 mM PBS (pH 7.4). (b) Signal suppression rate for background signal loss percentage of the SWV peak current as the function of time. (c) X-ray spectroscopy analysis (EDS) and scanning electron microscopy (SEM) of the rGO-AuNPs nanocomposite.

signal performed during biosensor optimization experiments (around 13%). This similarity between probable interfering compounds and background signal corroborates the selectivity and specificity of our platform in order to detect AR from biological samples and under a whole range of interfering compounds.

The literature states that the action of androgens is crucial for development of benign prostatic hyperplasia and prostate cancer; such behavior is mediated by the AR, which increases cellular proliferation when activated, and its role in prostate cancer cell is to promote the cancer progression [50]. In addition, the half-life of AR is sensitive to cellular microenvironment ranging from 3 hours to 10 hours in absence or presence of androgens [51]

Specifically for LNCaP cells lineage, the AR has an unusual high affinity for several steroids, even progestogens, which may explain the exacerbated proliferation of this cell type [52]. Given the importance of well-defined cancer monitoring tools, it is important to understand the correlation between the AR by different cell types and cancer aggressiveness [53]. The dynamics ruling AR can be different depending on prostate cell lineage tested. We herein selected two cell lines in order to provide a robust comparison and highlight the AR patterns, the PNT2, which is a normal prostate cell, and the LNCaP, which is an androgen-sensitive human prostate cancer cell [52, 54].

The AR monitoring patterns are shown in Figure 5. Figure 5(a) shows the SWV for PTN2 cells over time which by the end of the experiment was approximately 2 ng/mL (20% of SS) (Figure 5(b)) and can be comparable to AR concentration found on healthy patients [55]. On the other hand, the SWV pattern for AR on LNCaP (Figure 5(c)) suggests an overexpression of it with an approximately 50 ng/mL (55% of SS) (Figure 5(d)). The AR detection by the biosensor is aligned with the cell lineage type. LNCaP is an androgen-dependent lineage; therefore, we observed overexpression of

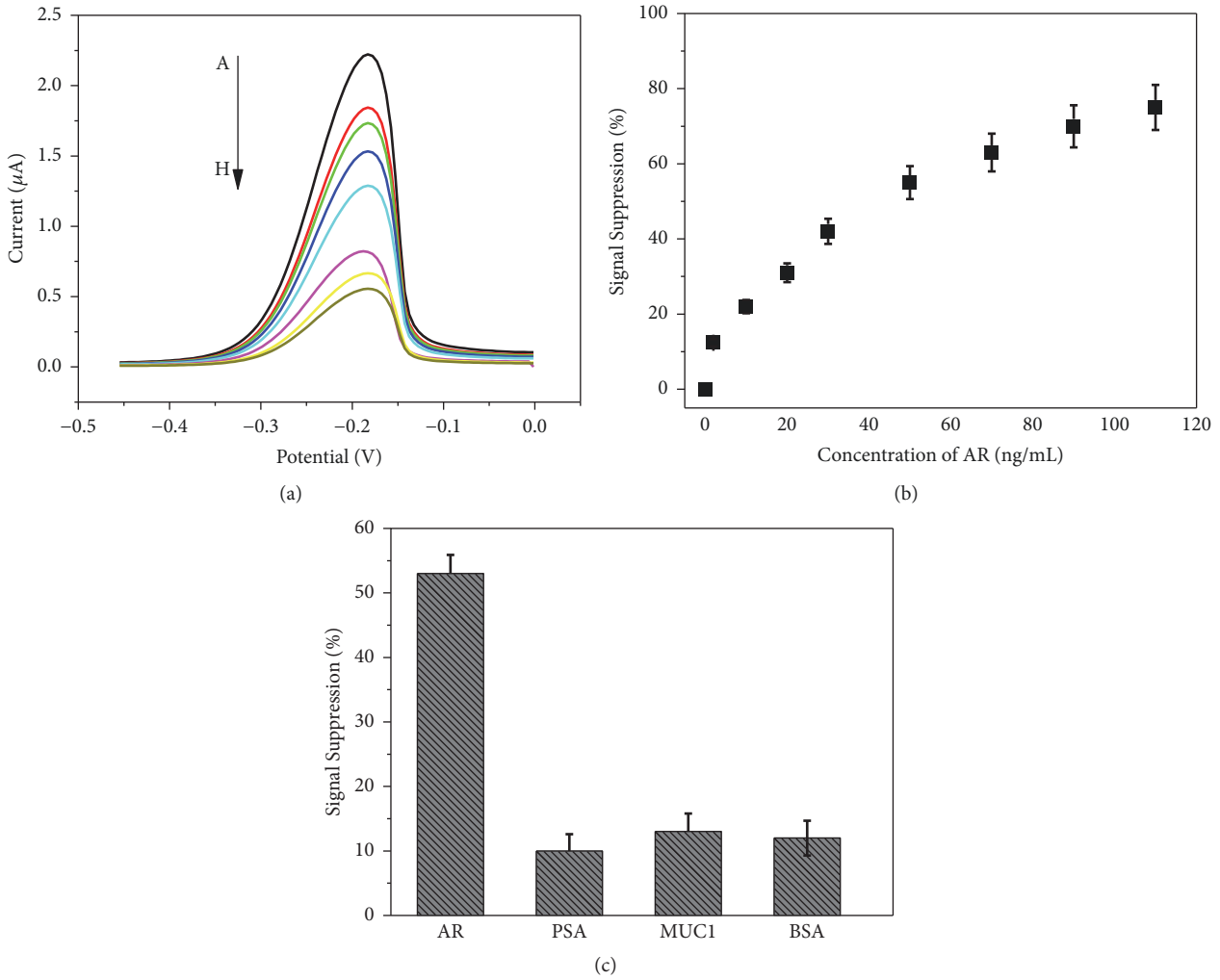

Figure 4: (a) Square wave voltammetry plot of the AR aptasensor at potential range 0.0 to -0.5 V, at 40 mV amplitude, and frequency 60 Hz—as AR concentration function (A-I: 0,2 10, 20, 30, 50, 70, 90, and 110 ng/mL), in 10 mM PBS buffer (pH 7.4). (b) Calibration plot of the PSA aptasensor showing signal suppression rate in signal loss percentage and SWV peak current as the function of several PSA concentrations. (c) Selectivity plot of aptasensor in presence of 50 ng/mL of AR, 50 ng/mL of PSA, 50 ng/mL of BSA, and 50 ng/mL of MUC1, showing signal suppression rate in signal loss percentage of SWV peak current.

AR and can be extrapolated in comparison to early-stage patients for PCa. In addition, the lower concentration of AR found for PNT2 lineage is in agreement with healthy patients and can be explained due to normal behavior of this cellular lineage [52].

The AR produced by prostate gland is vital to its normal development and function, and it is well known that the androgens play key role in the development and regulation of normal prostatic morphology and functions [56]. The AR is responsible for cellular proliferation, differentiation, and prevention of cell death; therefore, in prostate cancer cells the abnormal AR signaling leads to neoplastic cell proliferation and promotes cell survival [57]. Usually, for PCa diagnosis the PSA screening is the first exam, followed by digital rectal or biopsy [2, 5]; however, there is still a challenge regarding differentiating tumors that can be metastasize from benign ones and, in this way, the AR can be a powerful candidate to fulfill this gap.

In healthy cells, the epithelial AR normally produces proteins that will be secreted by prostate and the stromal AR is responsible for cellular growth; however, PCa cells cause changes in the stromal microenvironment leading it into a reactive stromal microenvironment [56], which will promote growth and signaling of cancer cells by activating a cascade of reaction and secretions of growth factors, such as growth factor β, vascular endothelial growth factor, insulin-like growth factor, fibroblast growth factor, and epidermal growth factor; thus the AR in prostate cancer will be a combination of normal signaling (PSA and lipid metabolisms) and abnormal growth promotions factors driving cancer cells to an exacerbated proliferation with promotion of cell survival [51, 58, 59].

AR patterns found by the aptasensor comply with the dynamics of AR reported in the literature, which can be associated with tumor aggressiveness and gene alterations. The PNT2 produced normal levels of AR, and LNCaP

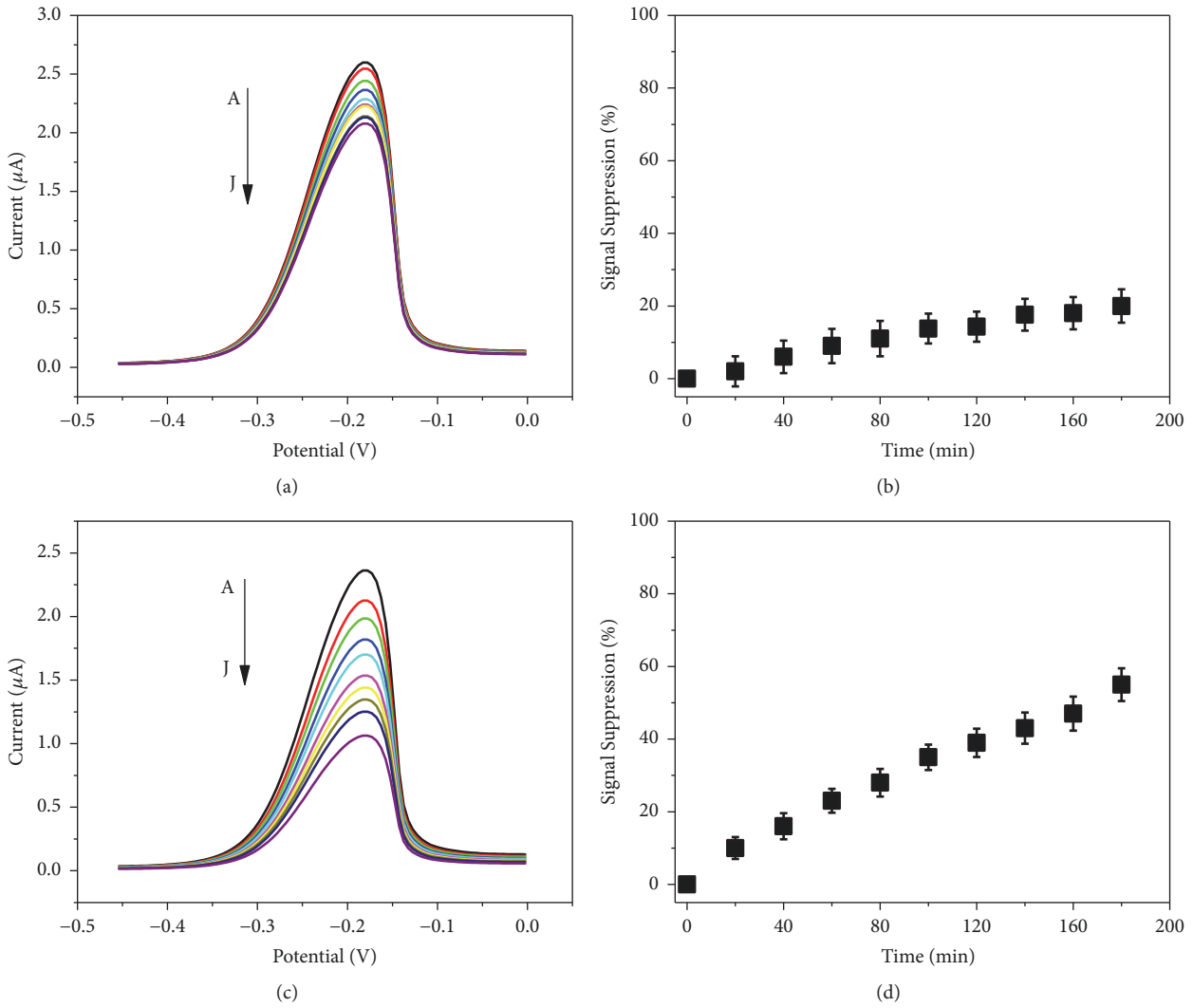

Figure 5: (a) Square wave voltammetry plot of the AR released by the PNT2 cell lineage at potential range 0.0 to -0.5 V, at 40 mV amplitude, and frequency 60 Hz over time in RPMI media. (b) Signal suppression rate in signal loss percentage of the SWV peak current as the function of AR produced by the PNT2. (c) Square wave voltammetry plot of the AR released by the LNCaP cell lineage at potential range 0.0 to -0.5 V, at 40 mV amplitude, and frequency 60 Hz over time RPMI media. (d) Signal suppression rate in signal loss percentage of the SWV peak current as the function of AR produced by the LNCaP line.

produced larger amounts of AR, and that can be linked with tumor aggressiveness, since the abnormal expression of AR leads to uncontrolled cellular growth and reduces cells apoptosis pathways [56, 57].

Therefore, our aptasensor clarifies the AR patterns production for different prostate cell lineages, and it provides a novel platform based on graphene oxide as an alternative to be applied to clinical samples for cancer monitoring; we hope in the near future it can be used to distinguish PCa from benign diseases.

4. Conclusion

The relationship between AR and prostate cancer progression has been exploited in clinical analysis as an attempt to improve the patient's survival rate. We developed a new electrochemical aptamer-based biosensor using reduced graphene oxide decorated with gold nanoparticles capable of monitoring the AR released by prostate cancer cells. The sensor recorded AR detection limits of 0.5 ng/mL, respectively, at linear range up to 100 ng/mL. It was also capable of detecting AR, even in the presence of several interfering compounds (PSA, BSA, and MUC1). By the integration of the high affinity between the aptamer and the cells, the as-designed biosensor can be used for highly sensitive protein release by cancer cells and dynamic evaluation of cell surface AR expression. In the near future, this biosensor can become a powerful clinical diagnostic instrument to detect PCa in its early stages.

Data Availability

The data used to support the findings of this study are included within the article.

Conflicts of Interest

The authors declare that they have no conflicts of interest.

Acknowledgments

This work was financially supported by the Brazilian agency FAPESP (2016/15919-8 and 2016/25749-2), CNPq, CAPES, Brazil.

References

[1] World Cancer Report 2014, *World Health Organization*, chapter 1.1, 2014.

[2] F. H. Schröder, J. Hugosson, M. J. Roobol et al., "Screening and prostate-cancer mortality in a randomized european study," *The New England Journal of Medicine*, vol. 360, no. 13, pp. 1320–1328, 2009.

[3] W. J. Catalona, J. P. Richie, F. R. Ahmann et al., "Comparison of digital rectal examination and serum prostate specific antigen in the early detection of prostate cancer: results of a multicenter clinical trial of 6,630 men," *The Journal of Urology*, vol. 151, no. 5, pp. 1283–1290, 1994.

[4] W. J. Catalona, D. S. Smith, and D. K. Ornstein, "Prostate cancer detection in men with serum PSA concentrations of 2.6 to 4.0 ng/mL and benign prostate examination: enhancement of specificity with free PSA measurements," *Journal of the American Medical Association*, vol. 277, no. 18, pp. 1452–1455, 1997.

[5] J. O. Ung, J. P. Richie, M.-H. Chen, A. A. Renshaw, and A. V. D'Amico, "Evolution of the presentation and pathologic and biochemical outcomes after radical prostatectomy for patients with clinically localized prostate cancer diagnosed during the PSA era," *Urology*, vol. 60, no. 3, pp. 458–463, 2002.

[6] L. T. Klein and F. C. Lowe, "The effects of prostatic manipulation on prostate-specific antigen levels," *Urologic Clinics of North America*, vol. 24, no. 2, pp. 293–297, 1997.

[7] C. Stephan, H. Cammann, H.-A. Meyer, M. Lein, and K. Jung, "PSA and new biomarkers within multivariate models to improve early detection of prostate cancer," *Cancer Letters*, vol. 249, no. 1, pp. 18–29, 2007.

[8] B. P. Crulhas, A. E. Karpik, F. K. Delella, G. R. Castro, and V. A. Pedrosa, "Electrochemical aptamer-based biosensor developed to monitor PSA and VEGF released by prostate cancer cells," *Analytical and Bioanalytical Chemistry*, vol. 409, no. 29, pp. 6771–6780, 2017.

[9] A. E. Karpik, B. P. Crulhas, C. B. Rodrigues, G. R. Castro, and V. A. Pedrosa, "Aptamer-based biosensor developed to monitor MUC1 released by prostate cancer cells," *Electroanalysis*, vol. 29, no. 10, pp. 2246–2253, 2017.

[10] Y. Niu, S. Altuwaijri, K. P. Lai et al., "Androgen receptor is a tumor suppressor and proliferator in prostate cancer," *Proceedings of the National Academy of Sciences*, 2008.

[11] C. S. Chang, J. Kokontis, and S. Liao, "Molecular cloning of human and rat complementary DNA encoding androgen receptors," *Science*, vol. 240, no. 4850, pp. 324–326, 1988.

[12] C. A. Heinlein and C. Chang, "Androgen receptor in prostate cancer," *Endocrine Reviews*, vol. 25, no. 2, pp. 276–308, 2004.

[13] N. Z. Lu, S. E. Wardell, K. L. Burnstein et al., "International union of pharmacology. LXV. The pharmacology and classification of the nuclear receptor superfamily: glucocorticoid, mineralocorticoid, progesterone, and androgen receptors," *Pharmacological Reviews*, vol. 58, no. 4, pp. 782–797, 2006.

[14] G. Schatzl, S. Madersbacher, A. Gsur et al., "Association of polymorphisms within androgen receptor, 5α-reductase, and PSA genes with prostate volume, clinical parameters, and endocrine status in elderly men," *The Prostate*, vol. 52, no. 2, pp. 130–138, 2002.

[15] D. Lee, W. Oh, and O. Sartor, "High androgen receptor levels are predictive of decreased survival in prostate cancer," *Clinical Prostate Cancer*, vol. 2, no. 1, pp. 13-14, 2003.

[16] A. A. Azad, S. V. Volik, A. W. Wyatt et al., "Androgen receptor gene aberrations in circulating cell-free DNA: biomarkers of therapeutic resistance in castration-resistant prostate cancer," *Clinical Cancer Research*, vol. 21, no. 10, pp. 2315–2324, 2015.

[17] M. Del Re, E. Biasco, S. Crucitta et al., "The detection of androgen receptor splice variant 7 in plasma-derived exosomal RNA strongly predicts resistance to hormonal therapy in metastatic prostate cancer patients," *European Urology*, vol. 71, no. 4, pp. 680–687, 2017.

[18] E. Michelini, P. Leskinen, M. Virta, M. Karp, and A. Roda, "A new recombinant cell-based bioluminescent assay for sensitive androgen-like compound detection," *Biosensors and Bioelectronics*, vol. 20, no. 11, pp. 2261–2267, 2005.

[19] M. Nesi, P. G. Righetti, M. C. Patrosso, A. Ferlini, and M. Chiari, "Capillary electrophoresis of polymerase chain reaction-amplified products in polymer networks: the case of Kennedy's disease," *Electrophoresis*, vol. 15, no. 1, pp. 644–646, 1994.

[20] S. A. Soper, K. Brown, A. Ellington et al., "Point-of-care biosensor systems for cancer diagnostics/prognostics," *Biosensors and Bioelectronics*, vol. 21, no. 10, pp. 1932–1942, 2006.

[21] I. Khalil, N. M. Julkapli, W. A. Yehye, W. J. Basirun, and S. K. Bhargava, "Graphene-gold nanoparticles hybrid-synthesis, functionalization, and application in a electrochemical and surface-enhanced raman scattering biosensor," *Materials*, vol. 9, no. 6, p. 406, 2016.

[22] A. K. Geim and K. S. Novoselov, "The rise of graphene," in *Nanoscience and Technology: A Collection of Reviews from Nature Journals*, pp. 11–19, 2010.

[23] C. A. Donini, M. K. L. da Silva, R. P. Simões, and I. Cesarino, "Reduced graphene oxide modified with silver nanoparticles for the electrochemical detection of estriol," *Journal of Electroanalytical Chemistry*, vol. 809, pp. 67–73, 2018.

[24] L. Wu, X. Lu, X. Fu, L. Wu, and H. Liu, "Gold nanoparticles dotted reduction graphene oxide nanocomposite based electrochemical aptasensor for selective, rapid, sensitive and congener-specific PCB77 detection," *Scientific Reports*, vol. 7, no. 1, article no. 5191, 2017.

[25] T.-K. Hong, D. W. Lee, H. J. Choi, H. S. Shin, and B.-S. Kim, "Transparent, flexible conducting hybrid multilayer thin films of multiwalled carbon nanotubes with graphene nanosheets," *ACS Nano*, vol. 4, no. 7, pp. 3861–3868, 2010.

[26] V. C. Tung, L.-M. Chen, M. J. Allen et al., "Low-temperature solution processing of graphene-carbon nanotube hybrid materials for high-performance transparent conductors," *Nano Letters*, vol. 9, no. 5, pp. 1949–1955, 2009.

[27] B. Huang, W. D. Zhang, C. H. Chen, and Y. X. Yu, "Electrochemical determination of methyl parathion at a Pd/MWCNTs-modified electrode," *Microchimica Acta*, vol. 171, no. 1-2, pp. 57–62, 2010.

[28] S. Stankovich, D. A. Dikin, R. D. Piner et al., "Synthesis of graphene-based nanosheets via chemical reduction of exfoliated graphite oxide," *Carbon*, vol. 45, no. 7, pp. 1558–1565, 2007.

[29] D. L. C. Golinelli, S. A. S. Machado, and I. Cesarino, "Synthesis of silver nanoparticle-graphene composites for electroanalysis applications using chemical and electrochemical methods," *Electroanalysis*, vol. 29, no. 4, pp. 1014–1021, 2017.

[30] I. Cesarino, R. P. Simões, F. C. Lavarda, and A. Batagin-Neto, "Electrochemical oxidation of sulfamethazine on a glassy carbon electrode modified with graphene and gold nanoparticles," *Electrochimica Acta*, vol. 192, pp. 8–14, 2016.

[31] S. Myung, A. Solanki, C. Kim, J. Park, K. S. Kim, and K.-B. Lee, "Graphene-encapsulated nanoparticle-based biosensor for the selective detection of cancer biomarkers," *Advanced Materials*, vol. 23, no. 19, pp. 2221–2225, 2011.

[32] X. Chen, X. Jia, J. Han, J. Ma, and Z. Ma, "Electrochemical immunosensor for simultaneous detection of multiplex cancer biomarkers based on graphene nanocomposites," *Biosensors and Bioelectronics*, vol. 50, pp. 356–361, 2013.

[33] G. Yang, Y. Yang, Y. Wang, L. Yu, D. Zhou, and J. Jia, "Controlled electrochemical behavior of indium tin oxide electrode modified with Pd nanoparticles via electrospinning followed by calcination toward nitrite ions," *Electrochimica Acta*, vol. 78, pp. 200–204, 2012.

[34] I. Cesarino, V. Cesarino, and M. R. V. Lanza, "Carbon nanotubes modified with antimony nanoparticles in a paraffin composite electrode: simultaneous determination of sulfamethoxazole and trimethoprim," *Sensors and Actuators B: Chemical*, vol. 188, pp. 1293–1299, 2013.

[35] I. Cesarino, H. V. Galesco, and S. A. S. Machado, "Determination of serotonin on platinum electrode modified with carbon nanotubes/polypyrrole/silver nanoparticles nanohybrid," *Materials Science and Engineering C: Materials for Biological Applications*, vol. 40, pp. 49–54, 2014.

[36] Y. Li, X. Fan, J. Qi et al., "Gold nanoparticles-graphene hybrids as active catalysts for Suzuki reaction," *Materials Research Bulletin*, vol. 45, no. 10, pp. 1413–1418, 2010.

[37] Y. Zhu, S. Murali, W. Cai et al., "Graphene and graphene oxide: synthesis, properties, and applications," *Advanced Materials*, vol. 22, no. 35, pp. 3906–3924, 2010.

[38] C. R. Basso, C. C. Tozato, B. P. Crulhas, G. R. Castro, J. P. A. Junior, and V. A. Pedrosa, "An easy way to detect dengue virus using nanoparticle-antibody conjugates," *Virology*, vol. 513, pp. 85–90, 2018.

[39] S. Zeng, K.-T. Yong, I. Roy, X.-Q. Dinh, X. Yu, and F. Luan, "A review on functionalized gold nanoparticles for biosensing applications," *Plasmonics*, vol. 6, no. 3, pp. 491–506, 2011.

[40] M.-C. Daniel and D. Astruc, "Gold nanoparticles: assembly, supramolecular chemistry, quantum-size-related properties, and applications toward biology, catalysis, and nanotechnology," *Chemical Reviews*, vol. 104, no. 1, pp. 293–346, 2004.

[41] B. Bohunicky and S. A. Mousa, "Biosensors: the new wave in cancer diagnosis," *Nanotechnology, Science and Applications*, vol. 4, no. 1, pp. 1–10, 2011.

[42] J. P. R. L. L. Parra, B. P. Crulhas, C. B. Rodrigues, F. K. Dellela, G. R. Castro, and V. A. Pedrosa, "Using an electrochemical aptasensor to early detect prostate specific and free prostate specific antigens released by cancer cells," *Electroanalysis*, vol. 30, no. 12, pp. 2869–2877, 2018.

[43] J. Yang, S.-X. Xie, Y. Huang et al., "Prostate-targeted biodegradable nanoparticles loaded with androgen receptor silencing constructs eradicate xenograft tumors in mice," *Nanomedicine*, vol. 7, no. 9, pp. 1297–1309, 2012.

[44] A. Balaji and J. Zhang, "Electrochemical and optical biosensors for early-stage cancer diagnosis by using graphene and graphene oxide," *Cancer Nanotechnology*, vol. 8, no. 1, p. 10, 2017.

[45] L. Feng, L. Wu, and X. Qu, "New horizons for diagnostics and therapeutic applications of graphene and graphene oxide," *Advanced Materials*, vol. 25, no. 2, pp. 168–186, 2013.

[46] M. Govindhan, M. Amiri, and A. Chen, "Au nanoparticle/graphene nanocomposite as a platform for the sensitive detection of NADH in human urine," *Biosensors and Bioelectronics*, vol. 66, pp. 474–480, 2015.

[47] S. Song, L. Wang, J. Li, C. Fan, and J. Zhao, "Aptamer-based biosensors," *TrAC Trends in Analytical Chemistry*, vol. 27, no. 2, pp. 108–117, 2008.

[48] B. P. Crulhas, D. Hadley, Y. Liu et al., "An electrochemical aptasensor for detection of bovine interferon gamma," *Analytical Methods*, vol. 9, no. 31, pp. 4527–4532, 2017.

[49] B. G. Mobbs, I. E. Johnson, J. G. Connolly, and J. Thompson, "Concentration and cellular distribution of androgen receptor in human prostatic neoplasia: Can estrogen treatment increase androgen receptor content?" *The Journal of Steroid Biochemistry and Molecular Biology*, vol. 19, no. 3, pp. 1279–1290, 1983.

[50] L. W. K. Chung, A. Baseman, V. Assikis, and H. E. Zhau, "Molecular insights into prostate cancer progression: The missing link of tumor microenvironment," *The Journal of Urology*, vol. 173, no. 1, pp. 10–20, 2005.

[51] E. D. Crawford, P. F. Schellhammer, D. G. McLeod et al., "Androgen receptor targeted treatments of prostate cancer: 35 years of progress with antiandrogens," *The Journal of Urology*, vol. 200, no. 5, pp. 956–966, 2018.

[52] D. K. Lee and C. Chang, "Endocrine mechanisms of disease: expression and degradation of androgen receptor: Mechanism and clinical implication," *The Journal of Clinical Endocrinology & Metabolism*, vol. 88, no. 9, pp. 4043–4054, 2003.

[53] J. Veldscholte, M. M. Voorhorst-Ogink, J. Bolt-de Vries, H. C. J. van Rooij, J. Trapman, and E. Mulder, "Unusual specificity of the androgen receptor in the human prostate tumor cell line LNCaP: high affinity for progestagenic and estrogenic steroids," *BBA - Molecular Cell Research*, vol. 1052, no. 1, pp. 187–194, 1990.

[54] S. A. Ingles, R. K. Ross, M. C. Yu et al., "Association of prostate cancer risk with genetic polymorphisms in vitamin D receptor and androgen receptor," *Journal of the National Cancer Institute*, vol. 89, no. 2, pp. 166–170, 1997.

[55] C. Mestayer, M. Blanchère, F. Jaubert, B. Dufour, and I. Mowszowicz, "Expression of androgen receptor coactivators in normal and cancer prostate tissues and cultured cell lines," *The Prostate*, vol. 56, no. 3, pp. 192–200, 2003.

[56] E. Giovannucci, M. J. Stampfer, K. Krithivas et al., "The CAG repeat within the androgen receptor gene and its relationship to prostate cancer," *Proceedings of the National Acadamy of Sciences of the United States of America*, vol. 94, no. 7, pp. 3320–3323, 1997.

[57] A. A. Shafi, A. E. H. Yen, and N. L. Weigel, "Androgen receptors in hormone-dependent and castration-resistant prostate cancer," *Pharmacology & Therapeutics*, vol. 140, no. 3, pp. 223–238, 2013.

[58] D. A. Barron and D. R. Rowley, "The reactive stroma microenvironment and prostate cancer progression," *Endocrine-Related Cancer*, vol. 19, no. 6, pp. R187–R204, 2012.

[59] M.-L. Zhu and N. Kyprianou, "Androgen receptor and growth factor signaling cross-talk in prostate cancer cells," *Endocrine-Related Cancer*, vol. 15, no. 4, pp. 841–849, 2008.